IEEE *Access*

Performance Evaluation of MIMO-FTN Signaling under Multipath Fading Channels

Hao-Tse CHIU[*], **Shuhei SAITO**[*] **Hirofumi SUGANUMA**[*], **Keita KURIYAMA**[†], **Kentaro TANAKA**[†], **Hitoshi HASEGAWA**[†], **Toshifumi MIYAGI**[†], **Takeshi ONIZAWA**[†], **and Fumiaki MAEHARA**[*]

[*]Graduate School of Fundamental Science and Engineering, Waseda University, Tokyo 169-8555, Japan
[†]NTT Access Network Service Systems Laboratories, Nippon Telegraph and Telephone Corporation, 1-1 Hikarino-oka, Yokosuka-shi, Kanagawa 239-0847, Japan

Corresponding author: Fumiaki Maehara (e-mail: fumiaki_m@waseda.jp).

ABSTRACT In this paper, we investigate the advantages of multiple-input multiple-output (MIMO) faster-than-Nyquist (FTN) signaling under a fixed utilized bandwidth and multipath fading channels. We present derivations of the input-output relationships for MIMO-FTN systems and decompose the MIMO transmission scheme into spatial and spectral precoding procedures. An approximated frequency-domain equalizer (FDE) is introduced at the receiver as an effective solution to decode the signals. The simulation results reveal that FTN signaling outperforms conventional Nyquist signaling under the fixed-bit transmission in terms of the bit error rate (BER) and throughput. It is shown that FTN signaling has the applicability of a lower-level modulation process, which might decrease the peak-to-average power ratio (PAPR), while there exists a tradeoff between PAPR and BER/throughput. Moreover, the advantages of the approximated FDE and FTN-SCFDE systems are confirmed in the MIMO configuration.

INDEX TERMS Faster-than-Nyquist (FTN) signaling, multiple-input multiple-output (MIMO), fixed-bit transmission, fixed utilized bandwidth, frequency domain equalization (FDE)

I. INTRODUCTION

IN recent years, the traffic demand for mobile broadband services has exponentially increased, and the standards for sixth-generation wireless communication (6G) are increasingly discussed [1], [2]. As a key capability, 6G systems are envisioned to provide extremely high peak data rates exceeding 1 Tbps [3]. To this end, a promising technique called faster-than-Nyquist (FTN) signaling has attracted increasing attention to achieve higher data rates and spectral efficiency since the 1970s [4]–[7]. Generally, the Nyquist pulse-shaping criterion [8] is frequently adopted to guarantee orthogonality and avoid inter-symbol interference (ISI) within data transmission. However, a guard band is required to ensure orthogonality, resulting in bandwidth efficiency loss.

In FTN signaling, ISI is intentionally allowed by sampling the data streams faster than the Nyquist rate [4], [5]. Since more non-orthogonal signals are transmitted, the data rate can be improved by breaking the orthogonality principle without expanding the bandwidth. Specifically, compared with conventional Nyquist signaling, the data transmission

of FTN signaling is performed under a compressed symbol period of $T = \zeta T_0$, where ζ symbolizes the compression factor (or symbol packing ratio), and T_0 represents the symbol interval that obeys the Nyquist criterion. Initially, FTN signaling was proposed to be applied to time-domain signals, and the following combination with single-carrier (SC) systems has become mainstream in FTN-related research over the past few decades [6], [7], [9]–[13]. Meanwhile, as a pioneering work, [14] introduced the concept of multicarrier FTN (MFTN) signaling, whose signals might experience ISI and/or inter-carrier interference (ICI) during transmission. The concept of MFTN gradually garnered the interest of researchers [14]–[17], which further highlights the flexibility of FTN signaling.

It is well-known that utilizing multiple antennas at the transceiver side is an effective method to obtain a higher transmission rate. Therefore, integrating the multiple-input multiple-output (MIMO) technique with FTN signaling has attracted significant attention naturally [10], [13], [18], [23]. In [23], the Mazo limit on a MIMO channel was investigated.

	MIMO	TX modulation scheme	multipath	colored noise	detection method
This paper	✓	SC, OFDM (MFTN)	✓	✓	FDE
[9]	✓(STMIM)	coded-SC	✓	✓	Gaussian MP
[10]	✓	SC	-	✓	- (capacity analysis)
[11]		SC	✓		FDE/ML
[12]		SC	✓	✓	FDE
[13]	✓	SC	-	✓	- (capacity analysis)
[18]	✓	SC	✓		iterative FDE
[19]	✓	SC	✓	✓	FDE
[20]		SC			decision feedback
[16]		MFTN	✓	✓	FDE
[17]	✓(IM)	MFTN	✓	✓	VAMP
[21]		NOMA	✓	✓	ML
[22]	✓	NOFDM			ML

TABLE 1: A brief comparison of the related FTN literature.

The authors in [10], [13] derived the capacity expressions and demonstrated the superiority of MIMO-FTN-SC systems. Reference [18] demonstrated the effectiveness of MIMO-FTN in terms of bit error rate (BER) and mutual information. Although the signal compression and multiple antennas lead to a greater transmission rate at the transmitter, the detection reliability degradation and the receiver complexity invoked by ISI become inevitable in the FTN systems.

It is challenging to design the detection algorithm for the receiver to recover the received signal in such a severe environment. Recently, numerous equalization and detection methods have been developed to eliminate the effects of ISI. We can briefly divide them into two main categories: (a) iterative algorithms [9], [11], [17], [18], [20]–[22], [24] and (b) one-tap equalizers [11], [12], [16], [19], [25]. For iterative methods, diversified algorithms are designed to decode the received signals. Examples include message passing-related algorithms [9], [17], maximum-likelihood (ML) estimation [11], [21], [22], and decision feedback algorithms [18], [20], [24]. On the other hand, one-tap equalizers based on classic zero-forcing (ZF) and minimum mean square error (MMSE) criteria are most commonly used. The equalizers in [11], [12] were developed based on the additive white Gaussian noise (AWGN) environment. However, especially for MMSE equalizers, which involves calculating the noise covariance matrix, the effect imposed by the colored noise from ISI should be introduced. Hence, [16], [19], [25] used approximated MMSE-frequency-domain equalizers (FDE) considering colored noise to enhance detection accuracy and reduce computational complexity. Owing to easy implementation and ease of simulation, this work adopts the one-tap MMSE-FDE at the receiver.

In addition, in previous MIMO-FTN studies, a single modulation scheme is usually assumed. In [9], a space-time multimode (STM) index modulation (IM) scheme with a Gaussian message passing (GMP)-based receiver was proposed to enhance the BER performance of an FTN-coded SC system given the same spectral efficiency and reduce the complexity compared with existing methods. In [17], another iterative method called the vector approximation message passing (VAMP) algorithm was applied to an IM-MFTN system. The results revealed the effectiveness of

the VAMP algorithm and IM-MFTN systems. In [22], experiments were conducted to demonstrate that FTN-non-orthogonal frequency division multiplexing (NOFDM) is promising under the MIMO scheme. Moreover, [19] adopted the MIMO-FTN systems employing SC-FDE, considering the impact of colored noise. According to our investigation, the comparisons between different modulation schemes are barely clarified.

Although enormous works have discussed FTN, some topics and investigations of MIMO-FTN systems remain open aside from the FTN literature. For instance, the restriction of the bandwidth expansion imposed by the pulse-shaping filter has been seldom concerned. Bandwidth resources are incredibly precious in realistic communication systems. Therefore, distinct from the aforementioned works that have generally determined a given bandwidth and accepted the excess generated by the pulse-shaping filter, we assume the total utilized bandwidth to be identical in this study, where it is also necessary to address the energy difference caused by the filter to achieve reasonable comparisons. Developing a more comprehensive system model to coordinate the present MIMO-FTN systems is another essential task.

Consequently, we summarize the necessary techniques into a MIMO-FTN precoded OFDM system model to include the FTN-SC and MFTN schemes together with the mathematical analyses. Additionally, we briefly compare some of the most related studies in Table 1. The major contributions of this study are as follows:

- A MIMO-FTN precoded OFDM system model is introduced to easily implement FTN-SC or MFTN systems by assigning the desired precoders. Comprehensive derivations of the overall MIMO effective channel matrix are also presented. We integrated several important techniques into a single system model concurrently.
- Approximated MMSE-FDE [16], [19], [25] is exploited to eliminate the ISI and colored noise effects in the equalization procedures at the receiver, which was first demonstrated to be compatible with MIMO systems in [19]. However, we provide more comparisons among higher-order modulation schemes, while merely QPSK is used in [19].
- To clarify the effect of FTN signaling, we mainly fo-

cus on the fixed-bit transmission, which represents the almost same spectral efficiency. Besides, extra simulations such as peak-to-average power ratio (PAPR) comparison and the effectiveness of MIMO configuration are also conducted.

- To conduct more practical simulations and achieve consistent spectral efficiency by the fixed-bit transmission, we fix the total occupied bandwidth in each case. Our results verify that MIMO-FTN systems can provide satisfactory performance in terms of BER, PAPR, and throughput under multipath fading channels.

The rest of the paper is organized as follows. The mathematical analyses of the MIMO-FTN precoded OFDM system model and the FDE considering the effect of the colored noise are described in Section II. In Section III, simulation results reveal the performance gains of SISO/MIMO-FTN systems under the multipath fading channel, especially for SC-FDE employing FTN signaling. Finally, concluding remarks are given in Section IV.

Notations: $\mathbf{x}$, $\mathbf{X}$, and x represent column vectors, matrices, and scalars, respectively. $\mathbf{X}^T$ and $\mathbf{X}^H$ denote the transpose and transpose-conjugate operation, respectively. The ith and (i,j)th entry of $\mathbf{x}$ and $\mathbf{X}$ is denoted by $[\mathbf{x}]_i$ $[\mathbf{X}]_{i,j}$, respectively. $|x|$ denotes the absolute value of x. $\circ$ and $\otimes$ symbolize the Hadamard and Kronecker products, respectively. For the expected value operator, $\mathbb{E}\{\cdot\}$ is used.

II. SYSTEM MODEL & ANALYSIS

A. MIMO-FTN PRECODED OFDM SYSTEMS

In this section, we construct a more general system model, a precoded OFDM system, to cover the difference between the FTN-SC and MFTN systems. The transceiver block diagram of a MIMO-FTN precoded OFDM system can be illustrated in Fig. 1. There are N_t transmit antennas and N_r receive antennas. In the p-th data stream ($0 \leq p \leq N_t - 1$), an N-length complex-valued modulated symbol vector $\mathbf{s}_p = [s_{p,0}, \cdots, s_{p,N-1}]^T \in \mathbb{C}^N$ with zero mean and unit variance is transmitted as the information bits. First, each symbol vector is precoded by the matrix $\mathbf{P}$ followed by an N-point inverse discrete Fourier transform (IDFT) matrix $\mathbf{F}_N^H$, whose (m,n)-th entry is defined as $e^{j2\pi mn/N}/\sqrt{N}$. To avoid inter-block interference (IBI), the cyclic prefix (CP) with length G is inserted in front of the information-bearing signal $\mathbf{x}_p$:

$$\mathbf{x}_{\text{cp},p} = \mathbf{A}_{\text{cp}}\mathbf{P}\mathbf{F}_N^H\mathbf{s}_p, \ \mathbf{A}_{\text{cp}} = \left[\begin{array}{cc} \mathbf{0}_{G\times(N-G)} & \mathbf{I}_G \\ \mathbf{I}_N \end{array} \right]. \quad (1)$$

After the CP insertion, a time-domain filter $g(t)$ pulse-shapes the $(N+G)$-length signal $\mathbf{x}_{\text{cp},p}$, where we assume $g(t)$ is a root-raised cosine (RRC) filter with a roll-off factor α and unit energy throughout this paper [26]. To achieve the FTN transmission, a symbol interval $T = \zeta T_0$ is set to generate the pulse-shaped FTN signal:

$$x_{\text{cp},p}(t) = \sum_{n=0}^{N+G-1} [\mathbf{x}_{\text{cp},p}]_n g(t - n\zeta T_0), \quad (2)$$

where T_0 is the minimum symbol interval under the Nyquist criterion and ζ, $0 < \zeta \leq 1$ represents the time-domain compression factor.

Between the p-th transmit antenna and q-th receive antenna ($0 \leq q \leq N_r - 1$), we assume each FTN signal streams experience a L-tap frequency-selective fading channel $\mathbf{h}_{q,p} \in \mathbb{C}^L$ with the channel coefficients $[\mathbf{h}_{q,p}]_l$ ($l = 0, 1, \cdots, L - 1$). At the receiver, a matched filter $g^*(-t)$ is adopted and the resultant signals are sampled at the interval T. Therefore, in the context of multipath fading channels, the matched-filtered signal of the q-th receive branch $y_q(t)$ can be represented as [19]

$$y_q(t) = \sum_{p=0}^{N_t-1} \sum_{l=0}^{L-1} \sum_n [\mathbf{h}_{q,p}]_l [\mathbf{x}_{\text{cp},p}]_n \gamma(t - (l+n)T) + \eta_q(t),$$

$$(3)$$

where

$$\gamma(t) = \int_{-\infty}^{\infty} g(\xi)g^*(t-\xi)d\xi, \ \eta_q(t) = \int_{-\infty}^{\infty} n_q(\xi)g^*(t-\xi)d\xi,$$

$$(4)$$

and $n_q(t)$ represents white Gaussian noise of q-th receive antenna with power N_0.

After the CP removal, the N-length received block $\mathbf{a} \in \mathbb{C}^N$ can be obtained as

$$\mathbf{a}_q = \sum_{p=0}^{N_t-1} \mathbf{R}_{\text{cp}}\mathbf{H}_{\text{ISI},q,p}\mathbf{x}_{\text{cp},p} + \boldsymbol{\eta}_q,$$

$$\mathbf{R}_{\text{cp}} = \left[\mathbf{0}_{N\times\frac{G}{2}} \quad \mathbf{I}_N \quad \mathbf{0}_{N\times\frac{G}{2}} \right], \quad (5)$$

where $\mathbf{R}_{\text{cp}}$ denotes the CP removal matrix, $\mathbf{H}_{\text{ISI},q,p} \in \mathbb{C}^{(N+G)\times(N+G)}$ represents the channel matrix including the effects of ISI induced by FTN signaling and the multipath fading, and $\boldsymbol{\eta}_q$ is the sampled version of $\eta_q(t)$. Specifically, the (k,m)-th entries of $\mathbf{H}_{\text{ISI}}$ can be calculated by

$$[\mathbf{H}_{\text{ISI},q,p}]_{k,m} = \sum_{l=0}^{L-1} [\mathbf{h}_{q,p}]_l \gamma(kT - (m+l)T). \quad (6)$$

Moreover, when the CP length is sufficiently long as $G > 2L$ and we assume $g(kT) = 0$, $|k| > \frac{G}{2}$, the approximated channel matrix $\mathbf{H}_{q,p,\text{approx}} = \mathbf{R}_{\text{cp}}\mathbf{H}_{q,p,\text{ISI}}\mathbf{A}_{\text{cp}}$ will become circulant, and the input-output relationship is given by [16]

$$\mathbf{a}_q \approx \sum_{p=0}^{N_t-1} \mathbf{H}_{q,p,\text{approx}}\mathbf{x}_p + \boldsymbol{\eta}_q. \quad (7)$$

With the aid of the circulant feature, $\mathbf{H}_{q,p,\text{approx}}$ can be diagonalized by the DFT matrix as $\mathbf{H}_{q,p,\text{approx}} = \mathbf{F}_N^H\boldsymbol{\Lambda}_{q,p}\mathbf{F}_N$. However, it is noteworthy that when the number of taps increases, $\mathbf{H}_{q,p,\text{approx}}$ will no longer be circulant. In such a condition, the off-diagonal terms in $\boldsymbol{\Lambda}_{q,p}$ appear and consequently worsen the detection reliability.
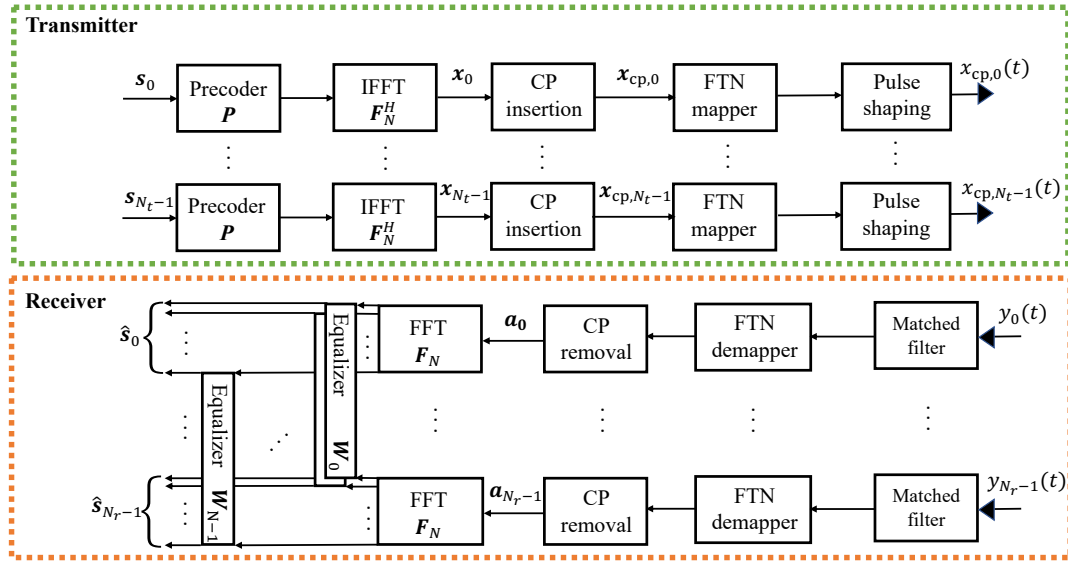
FIGURE 1: Illustration of the block diagram of the proposed FTN signaling system employing precoded OFDM.

B. FREQUENCY DOMAIN EQUALIZATION OF MIMO-FTN SYSTEMS CONSIDERING THE COLORED NOISE

Initially, we will emphasize the overall input-output relationship based on the MIMO systems. The precoding procedures can be divided into spectral and spatial modulation [27] as Fig. 2, corresponding to the frequency and spatial domain, respectively. According to the derivation in [27, Lemma 1], we can construct an overall effective channel matrix $\mathbf{H}_{\text{eff}}$ given by

$$\mathbf{H}_{\text{eff}} = \mathbf{W}_{\text{spec}} \circ (\mathbf{H}\mathbf{W}_{\text{spat}}) \tag{8}$$

where $\mathbf{W}_{\text{spec}} \in \mathbb{C}^{N_r N \times N_t N}$ represents the extended spectral precoding matrix, $\mathbf{H} \in \mathbb{C}^{N_r N \times N_t}$ denotes the collection of MIMO channels per-subcarrier, and $\mathbf{W}_{\text{spat}} \in \mathbb{C}^{N_t \times N_t N}$ is the assemblage of the spatial precoders.

In (8), $\mathbf{W}_{\text{spat}}$ is acquired by concatenating the spatially precoded matrices on the subcarrier-level by $\mathbf{W}_{\text{spat}} = [\mathbf{W}_{0,\text{spat}}, \cdots, \mathbf{W}_{N-1,\text{spat}}]$. In this study, we consider the case with $\mathbf{W}_{n,\text{spat}} = \mathbf{I}_{N_t}$, $n = 0, \cdots, N-1$ to simplify the analysis, where the comparisons between various spatial precoding schemes are left for future work.

On the other hand, coefficients in the spectral precoder will equivalently impose the effect to the $N_r \times N_t$ channel matrices for each subcarrier. Therefore, $\mathbf{W}_{\text{spec}}$ extends the precoding matrix $\mathbf{P}$ in (1) as

$$\mathbf{W}_{\text{spec}} = \mathbf{P} \otimes \mathbf{1}_{N_r, N_t} \tag{9}$$

where $\mathbf{1}_{N_r, N_t}$ denotes a $N_r \times N_t$ all-ones matrix. If we consider the SISO systems with $N_t = N_r = 1$, $\mathbf{W}_{\text{spec}}$ will reduce to $\mathbf{P}$.
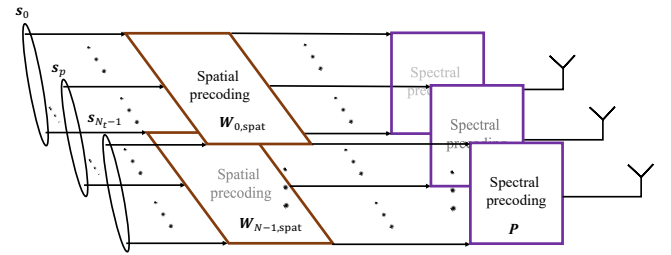

FIGURE 2: Illustration of the spatial and spectral precoding.

Finally, for the channel matrix $\mathbf{H}$, it is acquired by rearranging $\mathbf{\Lambda}_{q,p}$ based on the subcarrier index as

$$\mathbf{H}_n = \begin{bmatrix} [\mathbf{\Lambda}_{0,0}]_{n,n} & \cdots & [\mathbf{\Lambda}_{0,N_t-1}]_{n,n} \\ \vdots & \ddots & \vdots \\ [\mathbf{\Lambda}_{N_r-1,0}]_{n,n} & \cdots & [\mathbf{\Lambda}_{N_r-1,N_t-1}]_{n,n} \end{bmatrix} \in \mathbb{C}^{N_r \times N_t} \tag{10}$$

and all the channels per-subcarrier are further collected as $\mathbf{H} = [\mathbf{H}_0^T, \cdots, \mathbf{H}_{N-1}^T]^T$. Next, we define the overall input data vector $\mathbf{t} = [\mathbf{t}_0^T \cdots, \mathbf{t}_n^T \cdots, \mathbf{t}_{N-1}^T]^T \in \mathbb{C}^{N_t N}$, $\mathbf{t}_n = [s_{n,0}, \cdots, s_{n,N_t-1}]^T$ and similarly reshape the received signal $\mathbf{a}_q$, noise vector $\boldsymbol{\eta}_q$ as $\mathbf{r}, \boldsymbol{\eta}$. The transmission from $\mathbf{t}$ to $\mathbf{r}$ can be expressed as an overall single MIMO transmission:

$$\mathbf{r} = \mathbf{H}_{\text{eff}}\mathbf{t} + \boldsymbol{\eta}. \tag{11}$$

After constructing the input-output relationship, we would move on to equalization to recover the signal. The received signal is converted to frequency-domain via DFT and an overall FDE based on the MMSE criterion is adopted sub-

sequently [7], [25]:

$$\mathbf{W}_{\mathrm{MMSE}} =$$
$$\mathbf{H}_{\mathrm{eff}}^H(\mathbf{H}_{\mathrm{eff}}\mathbf{H}_{\mathrm{eff}}^H + \frac{1}{E_s}(\mathbf{F}_N^H \otimes \mathbf{I}_{N_r})\mathbb{E}[\boldsymbol{\eta}\boldsymbol{\eta}^H](\mathbf{F}_N \otimes \mathbf{I}_{N_r}))^{-1}. \quad (12)$$

where E_s represents the power of the transmitted signal. However, due to the data-compressing characteristic in FTN systems, the noise components at each receive antenna $\boldsymbol{\eta}_q$ will be colored, and the corresponding covariance matrices can be computed by

$$\mathbb{E}[\boldsymbol{\eta}_q\boldsymbol{\eta}_q^H] = N_0\boldsymbol{\Gamma} \in \mathbb{R}^{N \times N},$$
$$[\boldsymbol{\Gamma}]_{k,m} = \gamma((k-m)T), \quad (13)$$

which will also make the term $\mathbb{E}[\boldsymbol{\eta}\boldsymbol{\eta}^H]$ far from diagonal and induces high computation complexity. Note that for the cases of conventional Nyquist signaling, $\zeta = 1$ will lead to an identity noise covariance matrix ($\boldsymbol{\Gamma} = \mathbf{I}_N$), and the MMSE-equalizer has the well-known form as

$$\mathbf{W}_{\mathrm{white}} = \mathbf{H}_{\mathrm{eff}}^H(\mathbf{H}_{\mathrm{eff}}\mathbf{H}_{\mathrm{eff}}^H + \frac{N_0}{E_s}\mathbf{I}_{N_rN})^{-1}. \quad (14)$$

To ensure the subcarrier-wise operation in $\mathbb{E}[\boldsymbol{\eta}\boldsymbol{\eta}^H]$, we need to simplify $\mathbf{F}_N^H\mathbb{E}[\boldsymbol{\eta}_q\boldsymbol{\eta}_q^H]\mathbf{F}_N$ in (13). [7] proposed that the noise-related term can be approximated by a diagonal matrix $N_0\boldsymbol{\Phi}_q$ to reduce the computation loading, whose n-th diagonal entry is calculated by

$$[\boldsymbol{\Phi}_q]_n = \frac{1}{N}\sum_{k=0}^{N-1}\sum_{m=0}^{N-1} g((k-m)T)e^{(\frac{j2\pi(k-m)n}{N})}. \quad (15)$$

Finally, we can obtain the time-domain estimated symbol $\hat{\mathbf{t}}$ as the following equation and appropriate rearrangement follows behind if needed:

$$\hat{\mathbf{t}} = \mathbf{W}_{\mathrm{MMSE}}(\mathbf{F}_N \otimes \mathbf{I}_{N_r})\mathbf{r}. \quad (16)$$

III. SIMULATION RESULTS

In this section, we perform numerical simulations by MAT-LAB to verify the performance of MIMO-FTN systems under multipath fading channels. Since it has been proven that the RRC pulse-shaping filter induces $(1 + \alpha)$ times greater system bandwidth than that of the normal bandlimited communication systems [26], such the limitation of bandwidth should be included for fair and more practical comparisons. Different from some existing works that consider a given Nyquist bandwidth or even didn't highlight the bandwidth limit to transmit data [12], [13], [16], [17], [19]–[21], [28], [29], the total utilized bandwidth is fixed in our simulations. Precisely, the concept of the power spectrum can be illustrated in Fig. 3, which shows the effects of bandwidth extension along with the corresponding energy difference ensuring the consistent transmitted power caused by the various roll-off factors of the RRC filter.

Therefore, we assume the overall occupied bandwidth $2W = 2W'(1+\alpha) = 20$MHz, where the effective bandwidth $2W'$ is used for the Nyquist bandwidth in each case and
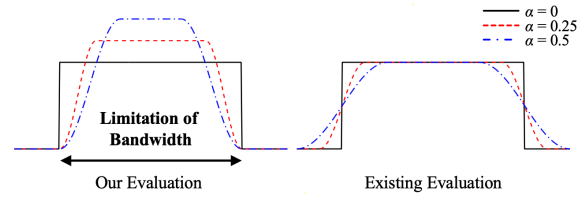

FIGURE 3: A schematic figure of the fixed bandwidth in this study.

the adjacent channel leakage power is almost 0 dB. Some related simulation parameters are summarized in Table 2. The constellation pattern for 16APSK is $[4, 12]$, of which 4 inner points are concentric with radius $r_0 = 0.5$, and inner/outer radius ratio = 2.57 [30]. Furthermore, we acquire the channel coefficients $[\mathbf{h}]_l$ of the L-tap fading channel with the distribution $\mathcal{CN}(0, 1/L)$ and assume the channel estimation is ideal. For more accurate results, we average the results of at least 5000 channel realizations.

Total Bandwidth	$2W$	20 (MHz)
Numbers of antennas	$N_t = N_r$	1, 2, 4
Data length	N	128
Modulation scheme	M	QPSK (M=4), 8PSK (M=8) 16QAM, 16APSK (M=16) cross 32QAM, 32PSK (M=32)
Cyclic prefix length	G	30
Pulse shaping filter		RRC, $\alpha = 0.25,\ 0.5$
Number of path	L	[1, 30]
Oversampling factor		10

**TABLE 2:** Related simulation parameters used in this study.

To evaluate the system performance, we mainly take bit error rate (BER) and system throughput as the performance metrics in this section. Here, we approximate the throughput by the binary entropy function $H(x) = -x\log_2 x - (1 - x)\log_2(1 - x)$ and the BER, which is given by [7], [19], [31]

$$\text{Throughput} = \frac{N}{N + G}\sum_{p=0}^{N_t-1} \frac{\log_2 M}{\zeta(1+\alpha)}(1 - H(P_{e,p})) \quad (17)$$

where M and $P_{e,p}$ denote the constellation size and the uncoded BER of the p-th stream obtained by the computer simulations, respectively.

A. PERFORMANCE COMPARISONS WITH DIFFERENT ROLL-OFF FACTORS

Fig. 4 provides the performance with the change of roll-off factor α and compressing factor ζ of SISO-SCFDE systems, where QPSK is assumed. In the simulations, we follow Fig. 3 assuming the total transmitted power is identical and define carrier-to-noise ratio (CNR) as CNR $= E_b/N_0 \times \log_2 M$ (dB). The BERs in Fig. 4(a) gradually deteriorate as ζ reduces because the ISI effects induced by symbol compression oppositely raise, where $\zeta = 1.0$ corresponds to the Nyquist signaling. Besides, it is observed that the case with $\alpha = 0.25$ has more significant degradation than that with $\alpha = 0.5$ due to the lower Mazo limit [4], [7]. In contrast, the curves in Fig. 4(b) prove that condensing the symbols does improve
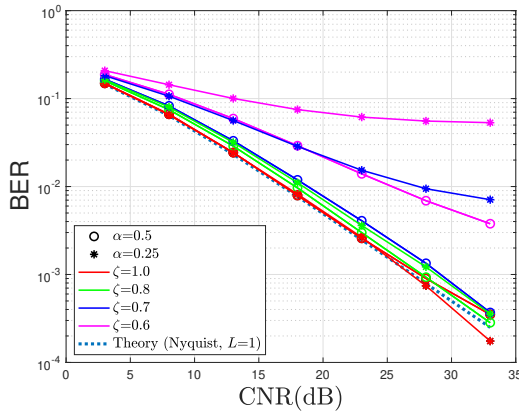
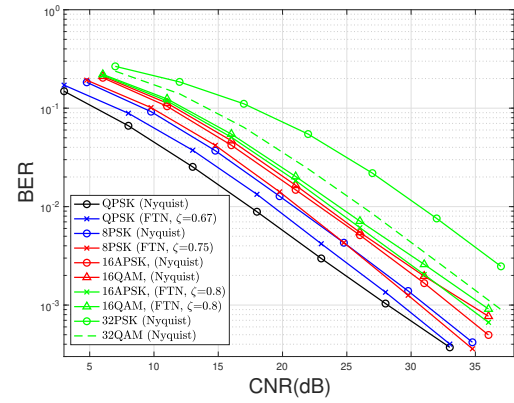**(a)** BER v.s. transmit carrier-to-noise ratio (CNR)
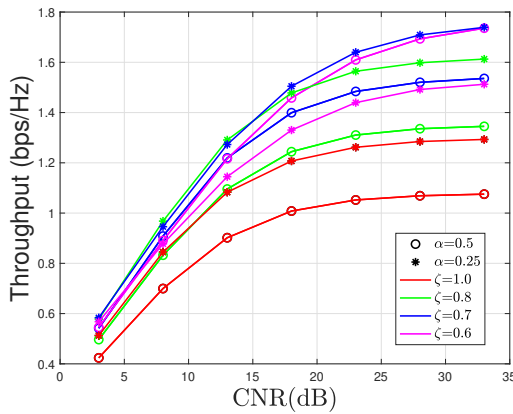
(b) System throughput v.s. transmit CNR

FIGURE 4: Transmission performance comparisons between different α and ζ of SISO-SCFDE systems with $L = 1$ and approximated FDE.
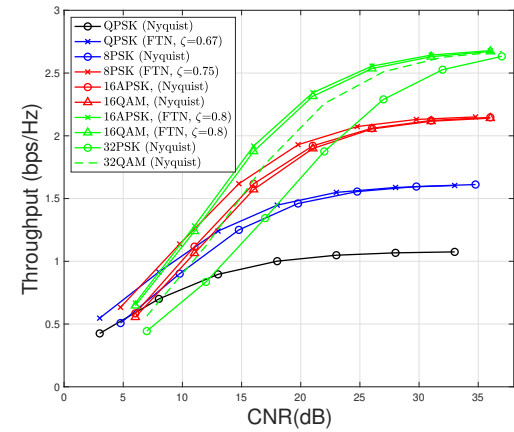

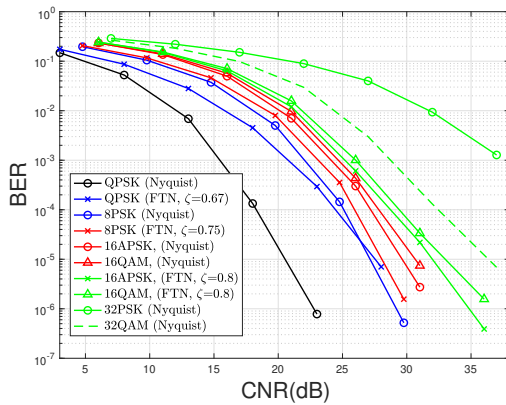**(a)** BER v.s. transmit CNR

(b) System throughput v.s. transmit CNR

FIGURE 5: Fixed-bit transmission performance comparisons of SISO-SCFDE systems with $L = 1$ and approximated FDE.

the throughput with BER degradation. However, although $\alpha = 0.25$ offers higher throughput until ζ diminishes to 0.7 thanks to the less bandwidth expansion, it results in worse BERs and the drop eventually flips the inclination when $\zeta = 0.6$. Based on these findings, in the following discussion, we would focus on the $\alpha = 0.5$ cases to allow a wider modifiable range of ζ with maintaining reasonable detection reliability.

B. FIXED-BIT TRANSMISSION OF SISO SYSTEMS

Next, we want to demonstrate the advantages of FTN over typical Nyquist signaling in SISO systems employing SC-FDE ($\mathbf{P} = \mathbf{F}_N$). Fig. 5 shows the BER and throughput in the context of a single path ($L = 1$), where the compressing factors are assigned based on the assumption of fixed-bit transmission. In this study, under the aforementioned assumption of fixed total bandwidth, fixed-bit transmission represents the transmission under the same spectral efficiency. For example, 3-bit transmission corresponds to Nyquist-8PSK and FTN-QPSK with $\zeta = 0.67$ decided by the factor $(\log_2 M)/\zeta$. In Fig. 5(a), it is evident that FTN signaling has superior detection reliability than Nyquist signaling in

most cases due to the utilization of lower-order modulation processes. For example, FTN-8PSK outperforms Nyquist-16APSK/16QAM and FTN-16APSK/16QAM accompany lower BER than Nyquist-32QAM.

Next, the system throughput results calculated by (17) are shown in Fig. 5(b). It can be observed that the outcomes will be asymptotic to $128/158 \times 1/1.5 \times \log_2 M/\zeta \approx 0.54 \times$ (bit number) and the cases with FTN signaling outperform Nyquist counterparts, especially in the low-CNR region. In 4-bit and 5-bit cases, FTN-8PSK and FTN-16APSK/16QAM lead to higher throughput while in the 3-bit case, a low compressing factor dilutes the BER difference between FTN-QPSK and Nyquist-8PSK. It is because FTN systems require squeezing the data symbol period more to achieve the transmission of an additional bit with the decrease of the transmitted bit, which increases the effects of ISI and leads to performance degradation.

Moreover, Fig. 6 shows the results of simulating the SISO SC-FDE systems under the multipath fading channels with $L = 30$ to reveal the effects of multipath fading. Here, distinct from the previous case that can perfectly meet the approximation (7) and avoid IBI, the number of paths is

(a) BER v.s. transmit CNR
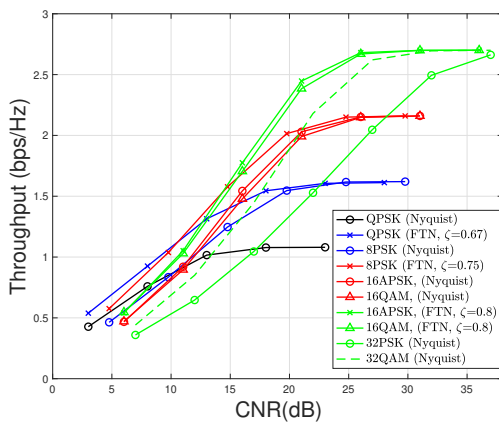
(b) System throughput v.s. transmit CNR

FIGURE 6: Fixed-bit transmission performance comparisons of SISO-SCFDE systems with $L = 30$ and approximated FDE.

set to be larger than $G/2$ on purpose. As we mentioned in Sec. II-A, the circulant feature no longer exists, and the off-diagonal terms in $\mathbf{\Lambda}_{0,0}$ appear as L increases. With such an extreme setting, we want to observe the interaction among degradation from IBI, multipath fading, and benefits from FTN signaling.

Similar to Fig. 5, FTN also outperforms Nyquist signaling and the gap moderately increases with the transmission bits. In higher-bit transmission (4 and 5-bit), the ISI influences more on the case with higher order modulation schemes due to their shorter minimum Euclidean distances (MED). However, under the multipath environments, FTN-16APSK/16QAM have larger performance gaps than Nyquist-32QAM/PSK thanks to the benefits of lower-order modulation and frequency diversity.

Fig. 7 shows the complementary cumulative distribution function (CCDF) of the PAPR. Based on Fig. 7, one can find that in 5-bit transmission, there is a tradeoff between BER and PAPR for FTN-16APSK/16QAM and Nyquist-32PSK/32QAM, which results from the 32PSK having
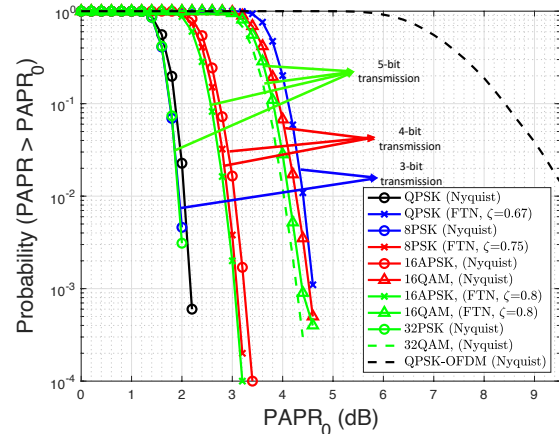

FIGURE 7: PAPR comparisons from 2 to 5-bit transmission with various modulation schemes employing FTN or Nyquist signaling.

shorter MED but almost unchanged amplitude levels compared with the 16APSK, while 16QAM/32QAM has the worst PAPR but satisfactory BER due to the rectangular-based shape. As for 4-bit cases, the PAPR of FTN-8PSK is slightly better than Nyquist-16APSK. The reason is that the modulation level can be reduced by squeezing the symbol period under the FTN criterion while retaining the transmission rate. Finally, when the 3-bit transmission is considered, although FTN-QPSK offers good detection performance, the PAPR performance is more terrible than Nyquist-8PSK. This phenomenon originates from the over-compressed symbol period might sample the pulse-shaping filter at more possible amplitude levels and invokes higher PAPR.

C. PERFORMANCE EVALUATIONS OF MIMO-FTN SYSTEMS

After demonstrating the advantages of SISO-FTN systems, we turn to investigate the performance of MIMO schemes. In this part, we conduct the simulations based on the analysis in Sec. II. For the parameter settings, we start from 2 transmit and receive antennas ($N_t = N_r = 2$) and take the orthogonal frequency division multiplexing (OFDM) scheme as a benchmark, where 16QAM is assumed. In addition, we reveal the effectiveness of the FDE considering the colored noise effect. In Fig. 8, we would like to divide the results into three topics: (a) solid and dash lines represent the difference between FDE with and without considering the colored noise, (b) colored lines show the system performance with different levels of compressing factor ζ, and (c) circle and triangle symbols denote two precoding matrices $\mathbf{P}$ in (1) ($\mathbf{P} = \mathbf{F}_N$ and $\mathbf{I}_N$), indicating SC-FDE and OFDM, respectively.

Firstly, from Fig. 8(a), approximated equalizers from (15) can alleviate the colored noise, and it is shown that the gap between two FDE methods is the largest when $\zeta = 0.7$, which results from more noticeable colored noise induced by FTN signaling in (13). Compared with FTN signaling cases, it is noteworthy that if $\zeta = 1$ (*i.e.,* Nyquist signaling), the FDE performance plots will overlap as we mentioned
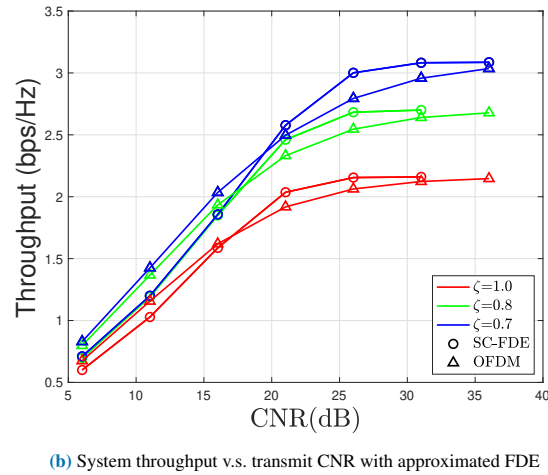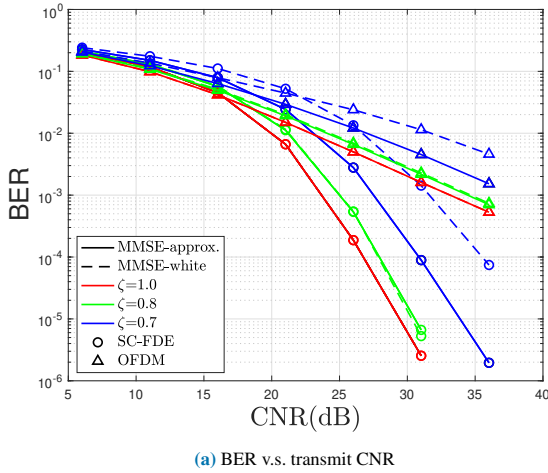
(a) BER v.s. transmit CNR

(b) System throughput v.s. transmit CNR with approximated FDE

FIGURE 8: Transmission performance of 2×2 MIMO-FTN with $L = 30$.

(a) BER v.s. transmit CNR

(b) System throughput v.s. transmit CNR

FIGURE 9: Transmission performance of SISO/MIMO-FTN systems with $N_t = N_r = 1, 2, 4$, $L = 30$ with approximated FDE.

in (14) of Sec. II-B. Secondly, we put our attention on the change in the compressing factor. One can observe that BER increases rapidly with the decrease in ζ because ISI becomes more serious, which is similar to Fig. 4. Next, since the compressing procedure in FTN-OFDM systems is performed in the frequency domain equivalently, we can observe that the BER performance deteriorates rapidly as ζ decreases because of the ICI. Besides, in both Nyquist and FTN signaling, cases utilizing MMSE-SCFDE outperform their MMSE-OFDM counterparts, especially in high-CNR regions. The benefits stem from the frequency diversity and the averaged subchannel error variance of MMSE-SCFDE [32, Chap. 6, 7].

Fig. 8(b) reveals the throughput performance of approximated FDE. The relationship between SC-FDE and OFDM is identical to the BER plot. Moreover, it is obvious that the signal compressing affects the value of throughput more significantly than BER does. Consequently, for FTN signaling, some sacrifice of the BER is inevitable to pursue higher data rates. In this case, we would say that $\zeta = 0.8$ provides better BER and satisfactory throughput while $\zeta = 0.7$ would be
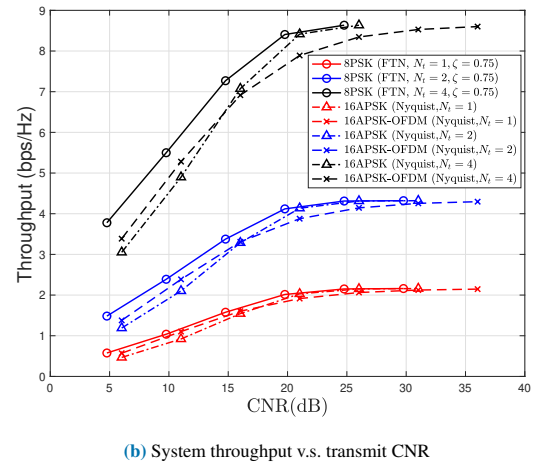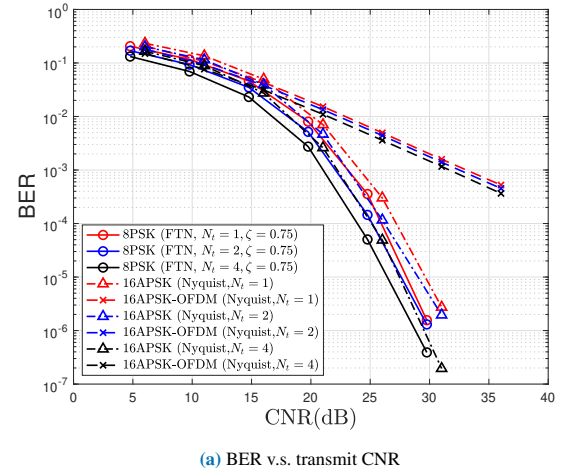
a preferable choice to obtain the highest throughput though some BER is sacrificed, where there is another tradeoff between BER and throughput.

D. INFLUENCE OF THE MIMO SCHEME ON THE FTN SIGNALING

Finally, we discuss the benefits of increasing the antenna number as shown in Fig. 9. We assume that there are 1, 2, or 4 antennas each at the transmitter and the receiver sides under the 4-bit transmission. In Fig. 9(a), it can be seen that BER performance improves with the increase in the antenna configuration because of the spatial diversity. The supremacy of FTN signaling over conventional Nyquist signaling and SC-FDE over OFDM has been verified again in MIMO settings. Note that for MIMO-FTN systems, it can be expected that as N_t (N_r) grows, the influence of colored noise might be more serious correspondingly, but the spatial diversity gain overcomes the degradation and results in the enhancement.

The throughput results are plotted in Fig. 9(b). In both 2×2 and 4×4 MIMO cases, FTN signaling prevails over Nyquist

signaling owing to the lower-order modulation process and compressed symbol sampling period. Moreover, the large number of data streams brings about a considerable throughput performance upturn compared with the SISO cases as expected.

E. SUMMARY OF SIMULATION RESULTS

In this subsection, we summarize the simulation results to highlight the observations in the simulation results. Our findings of each subsection in Sec. III are as follows:

- In Sec. III-A, we show the impact of α and ζ on the BER and system throughput. Lower ζ accompanies more ISI, which worsens the BER as expected but enhances the throughput. On the other hand, although lower α has the potential for higher throughput, the BER degradation is reckoned with.
- In Sec. III-B, the effectiveness of SISO-FTN over conventional Nyquist signaling is shown under frequency-flat and frequency-selective channels. The performance gap is more evident in the 5-bit transmission cases. Moreover, the tradeoff between PAPR and BER is revealed along with analyzing the supremacy of FTN signaling. Specifically, FTN-8PSK exhibits better performance than Nyquist-16APSK in both BER and PAPR.
- We discuss the numerical simulations of MIMO-FTN in Sec. III-C. The advantages of approximated FDE, the effect of the compressing factor, and the difference between FTN-SCFDE and FTN-OFDM (MFTN) are depicted. There might be a compromise between BER and throughput with the change of ζ in the signal transmission. Besides, FTN-SCFDE achieves satisfactory outcomes in contrast with FTN-OFDM, especially in high-CNR regions. Part of the results also fit the inclinations in [16], [19], [28].
- Sec. III-D simply demonstrates the gain acquired by the growing antenna number under multipath fading environments.

IV. CONCLUSION

In this study, we primarily investigated the system performance of SISO/MIMO-FTN-SCFDE systems, in which MFTN (FTN-OFDM) was also regarded as a benchmark. We presented a MIMO-FTN precoded OFDM system model and mathematical analyses. Specifically, the MIMO scheme was decomposed into spatial and spectral precoding procedures for compatibility with the system model. To eliminate the effect of ISI and colored noise, we used a one-tap approximated FDE to recover the signals. We fix the total utilized bandwidth in the simulations and considered the corresponding energy difference for more practical and reasonable comparisons. In both SISO and MIMO cases, the simulation results verified that FTN signaling has better BER and throughput performance under fixed-bit transmission. Moreover, the PAPR plot revealed the tradeoff between PAPR and BER/throughput and the capability to reduce the modulation level in FTN signaling. We demonstrated the

benefits of the approximated FDE and spatial diversity gain from MIMO under multipath fading channels.

REFERENCES

[1] M. Shafi, A. F. Molisch, P. J. Smith, T. Haustein, P. Zhu, P. De Silva, F. Tufvesson, A. Benjebbour, and G. Wunder, "5G: A tutorial overview of standards, trials, challenges, deployment, and practice," IEEE Journal on Selected Areas in Communications, vol. 35, no. 6, pp. 1201–1221, 2017.

[2] "White paper - 5G evolution and 6G," Japan, NTT Docomo Inc., White Paper, Jan. 2022.

[3] Z. Zhang, Y. Xiao, Z. Ma, M. Xiao, Z. Ding, X. Lei, G. K. Karagiannidis, and P. Fan, "6G wireless networks: Vision, requirements, architecture, and key technologies," IEEE Vehicular Technology Magazine, vol. 14, no. 3, pp. 28–41, 2019.

[4] J. E. Mazo, "Faster-than-Nyquist signaling," The Bell System Technical Journal, vol. 54, no. 8, pp. 1451–1462, Oct. 1975.

[5] J. B. Anderson, F. Rusek, and V. Öwall, "Faster-than-Nyquist signaling," Proceedings of the IEEE, vol. 101, no. 8, pp. 1817–1830, Aug. 2013.

[6] J. Fan, S. Guo, X. Zhou, Y. Ren, G. Y. Li, and X. Chen, "Faster-than-Nyquist signaling: An overview," IEEE Access, vol. 5, pp. 1925–1940, Feb. 2017.

[7] T. Ishihara, S. Sugiura, and L. Hanzo, "The evolution of faster-than-Nyquist signaling," IEEE Access, vol. 9, pp. 86 535–86 564, June 2021.

[8] S. Haykin, Communication Systems, 4th edition. New York: Wiley, 2001.

[9] S. Li, N. Wu, Q. Shi, and Q. Guo, "FTN signaling-aided space-time multi-mode index modulation systems with a GMP-based receiver," IEEE Access, vol. 7, pp. 162 898–162 912, 2019.

[10] M. Yuhas, Y. Feng, and J. Bajcsy, "On the capacity of faster-than-Nyquist MIMO transmission with CSI at the receiver," in 2015 IEEE Globecom Workshops (GC Wkshps), 2015, pp. 1–6.

[11] J. T. Wang, "Performance analysis for faster-than-Nyquist signaling under multi-path channel," IEEE Communications Letters, vol. 24, no. 2, pp. 302–306, 2020.

[12] S. Wen, G. Liu, C. Liu, H. Qu, L. Zhang, and M. A. Imran, "Joint precoding and pre-equalization for faster-than-Nyquist transmission over multipath fading channels," IEEE Transactions on Vehicular Technology, vol. 71, no. 4, pp. 3948–3963, 2022.

[13] Z. Zhang, M. Yuksel, and H. Yanikomeroglu, "Faster-than-Nyquist signaling for MIMO communications," IEEE Transactions on Wireless Communications, vol. 22, no. 4, pp. 2379–2392, 2023.

[14] F. Rusek and J. B. Anderson, "Multistream faster than Nyquist signaling," IEEE Transactions on Communications, vol. 57, no. 5, pp. 1329–1340, 2009.

[15] D. Dasalukunte, F. Rusek, and V. Owall, "Multicarrier faster-than-Nyquist transceivers: Hardware architecture and performance analysis," IEEE Transactions on Circuits and Systems I: Regular Papers, vol. 58, no. 4, pp. 827–838, 2011.

[16] T. Ishihara and S. Sugiura, "Reduced-complexity FFT-spread multicarrier faster-than-Nyquist signaling in frequency-selective fading channel," IEEE Open Journal of the Communications Society, vol. 3, pp. 530–542, Mar. 2022.

[17] Y. Ma, N. Wu, K. Wu, and J. A. Zhang, "VAMP-based iterative equalization for index-modulated multicarrier FTN signaling," IEEE Transactions on Communications, vol. 71, no. 4, pp. 2304–2316, 2023.

[18] M. McGuire, A. Dimopoulos, and M. Sima, "Faster-than-Nyquist single-carrier MIMO signaling," in 2016 IEEE Globecom Workshops (GC Wkshps), 2016, pp. 1–7.

[19] Y. Kumagai, A. Nakamura, S. Saito, H. Suganuma, K. Kuriyama, Y. Ono, H. Fukuzono, M. Yoshioka, and F. Maehara, "Performance improvement of faster-than-Nyquist single-carrier MIMO signaling considering the effects of colored noise," IEICE Communications Express, vol. 11, no. 4, pp. 176–182, Apr. 2022.

[20] T. Antsiferova, A. Ovsyannikova, A. Chudnov, and N. Dac Cu, "Comparison of FTN and Nyquist signaling in conditions of equal spectral efficiency," in 2022 International Conference on Electrical Engineering and Photonics (EExPolytech), 2022, pp. 195–198.

[21] P. Chaki and S. Sugiura, "Power-domain-multiplexed precoded Faster-than-Nyquist signaling for NOMA downlink," in GLOBECOM 2022 - 2022 IEEE Global Communications Conference, 2022, pp. 3977–3982.

[22] M. Guo, Y. Qiao, J. Zhou, X. Tang, J. Qi, S. Liu, X. Xu, and Y. Lu, "ICI cancellation based on MIMO decoding for FTN non-orthogonal FDM systems," Journal of Lightwave Technology, vol. 37, no. 3, pp. 1045–1055, 2019.

[23] F. Rusek, "On the existence of the Mazo-limit on MIMO channels," IEEE Transactions on Wireless Communications, vol. 8, no. 3, pp. 1118–1121, 2009.

[24] K. Wang, A. Liu, X. Liang, S. Peng, and Q. Zhang, "A faster-than-Nyquist (FTN)-based multicarrier system," IEEE Transactions on Vehicular Technology, vol. 68, no. 1, pp. 947–951, Jan. 2019.

[25] H. Fukumoto and K. Hayashi, "Overlap frequency domain equalization for faster-than-Nyquist signaling," Sept. 2015. [Online]. Available: https://arxiv.org/abs/1509.00562

[26] J. Anderson and A. Svensson, *Coded Modulation Systems*. Springer New York, 2003.

[27] R.-A. Pitaval and B. M. Popović, "Linear receivers for spectrally-precoded MIMO-OFDM," IEEE Communications Letters, vol. 21, no. 6, pp. 1269–1272, 2017.

[28] S. Sugiura, "Frequency-domain equalization of faster-than-Nyquist signaling," IEEE Wireless Communications Letters, vol. 2, no. 5, pp. 555–558, 2013.

[29] W. Yuan, N. Wu, H. Wang, and J. Kuang, "Variational inference-based frequency-domain equalization for faster-than-Nyquist signaling in doubly selective channels," IEEE Signal Processing Letters, vol. 23, no. 9, pp. 1270–1274, Sept. 2016.

[30] "Digital video broadcasting (DVB); second generation framing structure, channel coding, and modulation systems for broadcasting, interactive services, news gathering and other broadband satellite applications," European Telecommunications Standards Institute (ETSI), European Standard EN 302 307 V1.2.1, Apr. 2009.

[31] K. Kojima, Y. Shimbo, H. Suganuma, and F. Maehara, "Deep learning based CoMP transmission method using vehicle position information for taxi radio systems," in 2020 International Conference on Artificial Intelligence in Information and Communication (ICAIIC), 2020, pp. 253–256.

[32] Y.-P. Lin, S.-M. Phoong, and P. P. Vaidyanathan, *Filter Bank Transceivers for OFDM and DMT Systems*. Cambridge, U.K.: Cambridge Univ. Press, 2011.

HIROFUMI SUGANUMA Hirofumi Suganuma (Member, IEEE) received the B.Eng., M.Eng., and D.Eng. degrees from Waseda University, Tokyo, Japan, in 2016, 2018, and 2020, respectively. From 2020 to 2021, he was an Assistant Professor at School of Fundamental Science and Engineering, Waseda University. Since 2022, he has been engaged in the research and development of test and measurement systems at Anritsu Corporation, Kanagawa, Japan. Since 2023, he has also been an Adjunct Researcher at Waseda University. His current research interests include mobile communication systems. He is a member of IEICE.

KEITA KURIYAMA Keita Kuriyama received the B.E. and M.E. degrees in electronic engineering from Chiba University, Chiba, Japan, in 2015, 2017, respectively. Since joining Nippon Telegraph and Telephone (NTT) laboratories in 2017, he has been engaged in research and development of digital radio subscriber system and high reliable wireless system. He received the Young Researcher's Award from the the Institute of Electronics, Information and Communication Engineers (IEICE) in 2020.

HAO-TSE CHIU Hao-Tse CHIU received the B.S. and M.S. degrees in electrical engineering and communication engineering from National Taiwan University (NTU), Taipei, Taiwan, in 2017 and 2019, respectively. He is currently pursuing the Ph.D. degree with the Graduate School of Fundamental Science and Engineering of Waseda University, Tokyo, Japan. His current research interests include signal processing and optimization for wireless communication systems.

KENTARO TANAKA Kentaro Tanaka received the B.E. degrees in Information and Media technology engineering and M.E. in Fundamental Engineering for Knowledge Based Society from University of Fukui, Fukui, Japan, in 2020 and 2022, respectively. Since joining Nippon Telegraph and Telephone (NTT) laboratories in 2022, he has been engaged in research and development of radio frequency wireless communication.

SHUHEI SAITO Shuhei Saito (Member, IEEE) received the B.Eng., M.Eng., and D.Eng. degrees from Waseda University, Tokyo, Japan, in 2016, 2018, and 2021, respectively. He is currently an Assistant Professor with Waseda University. His current research interest includes mobile communications systems.

HITOSHI HASEGAWA Hitoshi Hasegawa received the B.Eng. degrees from Tohoku University, in 2007. He joined the NTT Access Network Service Systems Laboratories, in 2010, where he was engaged in the development of fixed wireless access systems.

This article has been accepted for publication in IEEE Access. This is the author's version which has not been fully edited and content may change prior to final publication. Citation information: DOI 10.1109/ACCESS.2023.3306797

IEEE *Access*

H. Chiu *et al.*: Performance Evaluations of single-carrier MIMO-FTN signaling under multipath fading channels

TOSHIFUMI MIYAGI Toshifumi Miyagi received a B.E. and M.E. in electronic engineering from Shibaura Institute of Technology, Tokyo, in 1995 and 1997. He joined NTT Wireless Systems Laboratories in 1997. Since then, he has been engaged in research and development of WLAN access systems, fixed wireless access systems, and terrestrial fixed systems. From 2013 to 2015, he was involved in regulatory and standardization activities for wireless systems. He is currently a senior research engineer, supervisor of NTT Access Network Service Systems Laboratories.

TAKESHI ONIZAWA Takeshi Onizawa received the B.E., M.E. and Ph.D. degrees from Saitama University, Japan in 1993, 1995 and 2003, respectively. Since joining NTT in 1995, he has been engaged in the research and development of personal communication systems, high data rate wireless LAN systems, future wireless access systems and radio propagation. He is currently an executive manager, executive research engineer of Wireless Entrance Systems Project, NTT Access Network Service Systems Laboratories. He is now in charge of management strategies of wireless communication systems. He received the best paper award, the young investigators award and the achievement award from IEICE in 2000, 2002 and 2006, respectively. He received the Maejima award in 2008. He also received the Best Paper Award in International Symposium on Antennas and Propagation (ISAP) in 2016 He is a senior member of the IEICE and a member of IEEE.
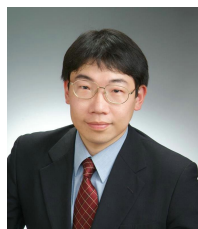
FUMIAKI MAEHARA Fumiaki Maehara (Senior Member, IEEE) received the B.Eng., M.Eng., and D.Eng. degrees from Waseda University, in 1993, 1995, and 2001, respectively. He joined the NTT Wireless Systems Laboratories, in 1995, where he was engaged in the research and development of personal communication systems. He was a Research Fellow at the Japan Society for the Promotion of Science (JSPS) and a Visiting Researcher at the Institute for Communications, University of Hannover, Germany, from 2003 to 2005. Since 2012, he has been a Professor with the Faculty of Science and Engineering, Waseda University. His current research interest includes mobile communication systems. He is a Senior Member of IEICE.

• • •